www.sciencemag.org/content/357/6355/1033/suppl/DC1

Supplementary Materials for

Behavioral time scale synaptic plasticity underlies CA1 place fields

Katie C. Bittner, Aaron D. Milstein, Christine Grienberger, Sandro Romani, Jeffrey C. Magee*

*Corresponding author. Email: mageej@janelia.hhmi.org

Published 8 September 2017, *Science* **357**, 1033 (2017)
DOI: 10.1126/science.aan3846

This PDF file includes:

Online Methods

All experiments were performed according to methods approved by the Janelia Institutional Animal Care and Use committee (Protocol 12-84 & 15-126).

Surgery and training

All *in vivo* experiments were performed in 6-12 week-old mice of either sex. All surgical procedures were performed under deep isoflurane or ketamine/xylazine anesthesia. After locally applying topical anesthetics, the scalp was removed, and the skull was cleaned. Then the skull was leveled and locations for the craniotomies for the whole-cell patch clamp and local field potential (LFP) recordings were marked using the following stereotactic coordinates: for the whole-cell recording 2.0 mm posterior from Bregma and 1.7 mm lateral from the midline; for the LFP recording 3.6 mm posterior from Bregma and 1.7 mm lateral from the midline. Then the skull was covered with super glue. As soon as the glue had dried custom-made titanium head bars with an opening over the hippocampus were attached to the skull using dental acrylic. 5-7 days after the head bar surgery running wheels were added to the home cages and mice were placed on water restriction (1.5 ml/day). After a period of 3-5 days of adapting the animals to being handled by the experimenter, animals were trained on the linear treadmill for 5-10 days. Mice were trained to run for a 10% sucrose/water reward delivered through a licking port once for every complete rotation of the belt (=lap of 180 cm). Mice were supplemented with additional water after training sessions to guarantee daily water intake of 1.5 ml/day. Mice were trained until the number of laps completed per day was similar for 2-3 days. The day prior to the first recording session the mice were anesthetized using isoflurane or ketamine/xylazine and two small (approximately 0.5 mm in diameter) craniotomies, one for the whole-cell patch electrode and one for the LFP electrode, were drilled at the previously marked positions. The dura was, if possible, left intact and craniotomies were covered with silicone elastomer.

Behavioral set up and control

The linear track treadmill consists of a belt made from velvet fabric that is enriched with visual and tactile cues as previously described[19,20]. The belt is self-propelled and divided up into three sectors enriched each with a different type of local cue. The sucrose/water reward was delivered through a custom-made lick port controlled by a solenoid valve. Photoelectric sensors were positioned at three locations on the belt and used to trigger the reward delivery, laser shutter, and current injections. The animal's speed was measured using an encoder attached to one of the wheel axles. The valve, sensors, and encoder were controlled with microprocessor-controlled behavioral control system interfaced with a Matlab GUI. A separate microprocessor interfaced with a Matlab GUI was used to control the laser shutter and current injections based on the animal's relative position on the belt.

In vivo electrophysiology

For each animal, the depth of the pyramidal cell layer was detected using the LFP. For this purpose, glass electrodes (1.5-3.5 MΩ) were filled with 0.9% NaCl. The extracellular electrode used to determine the pyramidal cell depth for whole cell recording was mounted vertically on a micromanipulator. The LFP signal was monitored using an audio amplifier and the electrode was advanced through the cortex. The pyramidal cell layer (typically 1.1-1.3 mm below the surface of the brain) was identified when theta modulated spikes were prevalent and the ripple amplitude increased. The extracellular electrode to be used for the simultaneous LFP recording during whole-cell patch clamp recordings was mounted on a second micromanipulator with a 40-45° angle relative to Bregma and advanced through the second more posterior craniotomy. This electrode was advanced until detection of the pyramidal cell layer and in some cases retracted ~50 μm along the same axis. To measure the phase shift between the LFP electrode location and the location of whole-cell patch recordings, we recorded the two LFP signals simultaneously. Whole-cell patch electrodes (7-12 MΩ) were filled with intracellular solution containing (in mM): 134 K-Gluconate, 6 KCl, 10 HEPES, 4 NaCl, 0.3 MgGTP, 4 MgATP, and 14 Tris-phosphocreatine. Liquid junction potentials were not corrected for. In some recordings, biocytin 0.2% was added to the intracellular solution. Whole-cell patch electrodes were advanced through the cortex with 6-8 psi of pressure. Upon entry into the hippocampus (approximately 100-200 μm from depth measured before using the extracellular electrode), the pressure was reduced to 0.25-0.35 psi. Cells were identified by reproducible increases in electrode resistance. All recordings were made in current clamp using an amplifier and digitized at 20 kHz. For the nimodipine experiments, the LFP electrode was filled with a solution containing 125 NaCl, 25 $NaHC0_3$, 3 KCl, 1.25 NaH_2PO_4, 1 $MgCl_2$, 1.3 $CaCl_2$, and 25 dextrose. This solution was bubbled for at least 30 minutes and then mixed with the vehicle or vehicle + drug (0.01% DMSO or 0.01%DMSO + 5uM nimodipine). As quickly as was possible (~15 minutes) this solution was loaded into the LFP electrode and lowered to the appropriate position. In cases where nimodipine was used the electrode was coated with Sharpie ink and the electrode holder covered with foil in order to prevent light induced breakdown of the drug.

In vitro electrophysiology

400 μm transverse hippocampal slices were cut using a vibratome from 6-9 week old male C57/Bl6 mice in a solution containing in mM: 210 Sucrose, 25 $NaHCO_3$, 2.5 KCl, 1.25 NaH_2PO_4, 0.75 $CaCl_2$, 7 $MgCl_2$, 7 Glucose. Slices were incubated for 30 mins at 35º C, and then recorded from at 35º C, in a solution containing: 125 NaCl, 25 $NaHC0_3$, 2.5 KCl, 1.25 NaH_2PO_4, 1 $MgCl_2$, 2.0 $CaCl_2$, and 25 dextrose. All solutions contained fresh Na pyruvate (3 mM) and ascorbic acid (1 mM), and were bubbled with 95% O_2 and 5% CO_2. Cells were visualized using an Olympus BX-61 microscope using a water-immersion lens

(40X, 0.8 NA, Olympus, Melville, NY). Whole cell current clamp recordings were performed in active "bridge" mode and analog-filtered at 1 kHz before being digitized at 50kHz. Whole-cell patch electrodes (6-8 MΩ) were filled with intracellular solution containing (in mM): 130 Cs-methanesulphonate, 6 KCl, 10 HEPES, 4 NaCl, 0.3 MgGTP, 4 MgATP, and 14 Tris-phosphocreatine. Liquid junction potentials were not corrected for. Series resistance was maintained between 20-45 MΩ in an attempt to allow proper filling with Cs^{2+} without overly dialyzing the neurons. We observed anecdotally in an initial set of recordings that plateau duration was relatively uncontrollable (durations >1 s) and that cell health (assessed by holding current values > 250 pA and Rin values less than 20 MΩ) and EPSP amplitude stability following plateau initiation were compromised in recordings where Rseries was less than 20 MΩ. Although difficult to quantify given the instability, it appeared that potentiation was likewise reduced. Trains of EPSPs were elicited by electrically stimulating (0.1 ms, 0.1-0.5 mA) axons in the *Str. radiatum* using tungsten microelectrodes (12 MΩ) placed ~200-400 μm away from the recording site. Input resistance was measured using a 50 ms, -25 pA current injection following the EPSP test stimulation. Nimodipine was dissolved at 10 mM as a stock solution in ethanol and then further diluted to 10 μM by addition of external solution. Nimodipine containing solutions were protected from room light. D-APV (20 μM) and Gabazine (1-2 μM) were dissolved directly into external solutions.

Data analysis

Naturally occurring place field induction was detected as the sudden appearance of position specific firing (generally appearing within a single lap; see below for definition) after a number of trials (>10 laps) in which no position dependent firing was present. V_m traces from the trials immediately preceding the sudden appearance of PF firing were examined for plateau potentials.

To analyze ramps of depolarization (V_m ramp) APs were removed by deleting all points 0.26 ms before and 3.4 ms after a threshold value (d V_m /dt = 50 V/s) and the resulting trace was low-pass filtered (<3 Hz) using an FIR filter with a 200 ms Hamming window. Individual V_m ramp traces were subsequently binned (100 equal sized spatial bins) and averaged for time periods covering from 5-10 mins. Ramp amplitude was quantified as the difference between peak (10 cm average around most depolarized value) and the baseline (20 cm average around most hyperpolarized value). Ramp width was determined as the distance between positions where ramp V_m amplitude as 0.15 of the peak. The average velocity of the mouse was calculated from the V_m ramp start (position where ramp amplitude was 0.15 of peak) to ramp end (position where ramp amplitude decayed to 0.15 of peak). Single trials were used for the naturally-induced place fields and the three trials exhibiting the fastest velocities were averaged for the experimentally-induced place fields. The speed dependence of V_m ramp width was determined by average the V_m ramps for the 5 slowest trials and for the 5 fastest trials following the place field induction, with the

criterion that the fastest trials had to be at least twice the average velocity of the slowest trials. This criterion was met for 22 of the 27 neurons in the population.

The firing fields of single neurons were determined by first dividing the length of the belt into 100 bins. For each bin, the number of APs discharged in the bin was divided by the time the animal spent in the bin in order to generate a vector of firing rates. The firing rate vector was smoothed by a running average (boxcar) of 5 bins. Periods when the mouse ran slower than 5 cm/s were removed from analysis. Neurons were considered place cells if the firing rates of a series of the adjacent bins was 0.2 of the peak for at least 20 cm (10 bins) and had a mean in-field firing rate more than 3 times larger than the mean out-of-field firing rate. Plateau duration determined as amount of time V_m spent more depolarized than -30 mV during the 300 ms current injection.

Synaptic plasticity rule – inference from data

We assumed that changes in synaptic weights $W(z)$ between a plateau potential emitting CA1 cell and a simulated CA3 place cell with preferred location z were linearly accumulated during induction trials[7]

$$W(z) = W_0(z) + \alpha \sum_{t,t'=0}^{T} R_{CA1}(t')K(t'-t)R_{CA3}\big(z - x_A(t)\big), \qquad (1)$$

where $W_0(z)$ denotes a pre-induction synaptic weight, α is a constant post-synaptic dependent learning rate, $R_{CA1}(t')$ is a binary function that takes the value 1 during a plateau potential (300ms duration for induced plateaus), and 0 otherwise. The firing rate of CA3 cells is characterized by the function $R_{CA3}(x)$, peaking at $x = 0$ and decaying monotonically away from $x = 0$. The firing rate profile $R_{CA3}\big(z - x_A(t)\big)$ mimics the firing time course of a CA3 place cell with preferred location z when the animal is moving according to the trajectory $x_A(t)$, measured experimentally. The unknown kernel $K(t'-t)$ modulates the synaptic weight changes depending on the activity of the post (pre)- synaptic cells at time $t'(t)$, respectively. The experiment runs from time 0 to T, time is discretized in steps of $15ms$.

We also assumed that the spatial profile of the membrane potential of a CA1 cell post-induction, $V_m(x)$, is a linear combination of the pre-synaptic firing rate weighted by the learned synaptic weights

$$V_m(x) = \sum_{z=0}^{L} W(z)\, R_{CA3}(z - x), \qquad (2)$$

where L denotes the length of the circular track (187cm), discretized in $10cm$ steps. By substituting the expression for the learned synaptic weights (Eq 1) in Equation 2, we obtain

$$\Delta V_m(x) = V_m(x) - V_m^0(x) = \alpha \sum_{t=0}^{T} H(t)\tilde{R}_{CA3}\big(x - x_A(t)\big). \qquad (3)$$

Here $V_m^0(x) = \sum_{z=0}^{L} W_0(z)R_{CA3}(z-x)$ is the V_m spatial profile before induction, which

was either measured when data was available, or assumed to be the minimum of the post-induction V_m ramp otherwise. $H(t) = \sum_{t'=0}^{T} R_{CA1}(t')K(t'-t)$ denotes the plateau potential time-course convolved with the plasticity kernel and $\tilde{R}_{CA3}\big(x - x_A(t)\big) = \sum_{z=0}^{L} R_{CA3}(z-x)R_{CA3}\big(z - x_A(t)\big)$ is the firing rate profile of symmetric CA3 place fields convolved with itself. For the case of a Gaussian place field of width σ, the resulting shape would be Gaussian of width $\sqrt{2}\sigma$.

The linearity assumptions for the synaptic weights modifications and the linear relation between post-synaptic V_m and pre-synaptic firing result in a linear equation relating the unknown plasticity kernel (in H(t)) and the measured V_m ramp together with the measured animal trajectory (Eq 3). The remaining assumption concerns the shape of CA3 firing, which we assumed to be a Von Mises function with concentration parameter $k = 2, \tilde{R}_{CA3}(x) = \exp(k\, cos(\frac{2\pi}{L}x))$. The CA3 firing rate was further baseline-shifted and peak-normalized to a [0,1] range. We solved the linear equation (Eq 3) by estimating the pseudo-inverse of the CA3 firing rate matrix, employing a Tikhonov regularization; We first computed the SVD of the CA3 matrix (indexed by x and t), $\tilde{R}_{CA3}\big(x - x_A(t)\big) = U\, S\, V^T$ and estimated its inverse as $\tilde{R}^{-1}{}_{CA3}\big(x - x_A(t)\big) = V\, D\, U^T$, where $D_{ii} = \frac{S_{ii}}{S_{ii}+\beta^2}, \beta = 15$. This procedure resulted in a smooth least-square estimate (up to a rescaling factor) of $H(t)$ denoted by $\widehat{H}(t) \propto \sum_{x=0}^{L} \Delta V_m(x)\, \tilde{R}^{-1}{}_{CA3}\big(x - x_A(t)\big)$. In Fig. 2 we report this estimate for single cells, centered around the plateau induction onset and averaged across the induction trials in a time window of [-5,5] s – the synaptic rule. For comparison across cells, we normalized each synaptic rule from individual cells with its average in the [-5,5] s window, and computed the mean across cells (Fig 2). Similar results were obtained following normalization with the peak value of the synaptic rule, or no normalization (Fig S4a). We explored the robustness of the method by varying the two available free parameters, the regularization parameter β and the concentration parameter k (Fig S4b). We observe that our choice of concentration parameter, reproducing the typical size of place-field firing in dorsal CA3[23], accounts for the observed variability of V_m ramp width across cells (Fig S4b).

Estimate of V_m ramp spatial properties

We further estimated the spatial properties of the V_m ramps under the simplifying assumptions of a virtual rodent running in a long (compared to place field size) linear track at constant speed v, $x_A(t) = v\, t$. The plasticity kernel is assumed to have the exponential form $K(t) = e^{-\frac{t}{\tau_b}}\theta(t) + e^{\frac{t}{\tau_f}}\theta(-t)$, with backward and forward time constants (see Fig 3g) denoted by τ_b and τ_f respectively, where $\theta(t)$ is the Heaviside function. We also assumed that CA3 place field firing is described by a Gaussian of standard deviation σ. With a continuous approximation of Eqs. 1 and 2 it is possible to analytically estimate the spatial depolarization profile of an ideal CA1 cell, $V_m(x)$, resulting from an instantaneous plateau

potential $R_{CA1}(t) = \delta(t)$ occurring when the animal is at location $x_A(0) = 0$. In particular, the center of mass of the ramp, $\frac{\langle xV_m(x)\rangle}{\langle V_m(x)\rangle}$, where $\langle\cdot\rangle$ denotes spatial averaging, is

$$\frac{\langle xV_m(x)\rangle}{\langle V_m(x)\rangle} = v(\tau_f - \tau_b)$$

resulting in a center of mass location that is predictive of the location at which the simulated plateau occurred (Fig S9). Given the experimentally measured values of forward and backward time constants, the center of mass shift would approximately be 30 cm for a mouse running at 50 cm/s. In a similar manner, we can estimate the variance of the V_m spatial profile,

$$2\sigma^2 + v^2({\tau_f}^2 + {\tau_b}^2)$$

and its skewness,

$$\frac{2v^3({\tau_f}^3 - {\tau_b}^3)}{(2\sigma^2 + v^2({\tau_f}^2 + {\tau_b}^2))^{3/2}}.$$

Parametric fitting of dual component synaptic plasticity rule to data

The ramp depolarization of a CA1 place cell was assumed to result from the weighted sum of the firing rates of CA3 place cell inputs, convolved with an EPSP-shaped kernel (τ_{rise}: 5 ms, τ_{decay}: 20 ms). CA3 place cell firing rates were spatially modulated with a 90 cm field width, temporally modulated with theta frequency (~6.7 Hz) during running, and phase precessing relative to extracellular theta[20]. For each cell in the experimental dataset, the rise and decay time courses of a local synaptic kernel and a global dendritic kernel were optimized to produce a distribution of synaptic weights that recapitulates the shape and amplitude of the observed V_m ramp, given the variable running speed of the animal, and variable onset locations and durations of plasticity-inducing current injections or spontaneous plateaus (Fig. S5). Input firing rates were set to zero when run velocity was less than 5 cm/s. Basinhopping and simplex algorithms were employed to minimize an error function based on the amplitude of the V_m ramp in 100 spatial bins, the ramp width, the peak location of the ramp relative to plateau onset, and the ratio of rising and decaying phases of the ramp (Fig. 2H). The long time scale plasticity rule was parameterized by the following six bounded parameters: local τ_{rise} (10-500 ms), local τ_{decay} (500-5000 ms), global τ_{rise} (10-30 ms), global τ_{decay} (100-2000 ms), and relative ratio of global and local signal amplitudes (0.75-1.5) (Fig. S5). For the short time scale plasticity rule, local and global kernel time scales were imposed (local and global τ_{rise}: 10 ms, local and global τ_{decay}: 100 ms). The resulting local kernels were convolved with the compound EPSP waveforms for each input, and the global kernels were convolved with the square current injection or spontaneous plateau waveforms. The amount to increment the synaptic weight of each input during each induction trial was determined by the area of overlap between the resulting local and global signals. Saturation of induced synaptic weights occurred in some cells when the optimal ratio of global to local kernel amplitudes was below

one. Finally, synaptic weight distributions generated by this procedure were used to drive CA1 place field activity in more biophysically realistic simulations with discrete spike trains activating synaptic inputs with stochastic release probability, voltage compartmentalization in spines and dendrites expressing voltage-dependent conductances, and synaptic inhibition gating nonlinear dendritic integration[20]. Numerical simulations were implemented using custom software extending the Python interface for the NEURON simulation environment[37]. All code is publicly available on GitHub[38]. During simulated traversal of a linear track treadmill with wraparound, ~1425 CA3 and ~175 ECIII excitatory inputs containing AMPA-Rs and NMDA-Rs were activated according to their spatial and temporal tuning, and ~600 inhibitory inputs containing GABA(A)-Rs were activated without spatial tuning. The resulting ramp depolarizations were filtered and analyzed identically to the experimental data.

Statistical methods

No statistical methods were used to predetermine sample sizes. Where appropriate, data were analyzed using two-tailed paired or unpaired *t*-tests, as stated in the text or figure legends. If normality was uncertain, we used non-parametric test as stated in the text or figure legends. Data are shown as mean ± SEM. Means and P-values in Figure 3 are -3250 ms: 1.26±0.06, p=0.129; -1250 ms: 1.74±0.11, p=0.001 (*); -750 ms: 2.16±0.143 p=0.0005 (*); -250 ms: 2.67±0.15, p=1.08e-4, n=7 (*); 0 ms: 3.12±0.11, p=1.5e-5, n=4(*); +250 ms: 2.3±0.17, p=0.0039, n=4(*); =550-+750 ms: 1.65±0.08, p=0.004; +850-+2250 ms: 1.39±0.07, p=0.06.

Supplementary figure legends

Fig. S1. Measurement of V_m **ramp properties and values. A)** Representative V_m ramp showing how various values are calculated. **B)** Population data for rise and decay V_m ramp width. **C)** Ratio of rise and decay widths showing asymmetry in V_m ramp. **D)** V_m ramp amplitudes. **E)** distance between the position of the leading edge of the plateau and the peak of the V_m ramp. Grey symbols indicate neurons with experimentally-induced ramps, red symbols are neurons with naturally-occurring ramps. No significant differences were observed in any measured values for naturally occurring versus experimentally induced V_m ramps. **F**) table listing mean±sem values and p-values from paired two-tailed T tests for all neurons, experimentally-induced and naturally occurring plateau.

Fig. S2. Measurement of times and velocities associated with V_m **ramp. A)** V_m of trial with spontaneous plateau. Time of the event indicated. **B)** V_m ramp determined from subsequent trials showing the start and end positions of the ramp (red crosses) as well as the position of the plateau (grey line). **C)** position in time of the mouse during the above trial showing the start and end time (red crosses) of the ramp. Backward and forward times indicated by arrows. **D)** velocity versus time of mouse on above trial showing the start and end times of the ramp (red lines). Region of the velocity profile used to calculate the average velocity of the mouse indicated by arrows and average velocity, as used in Figure 1, is shown.

Fig. S3. Comparison of observed and inferred V_m **ramps of individual place cells. A)** Experimental V_m ramps with baseline subtracted, spatially shifted to center the place field maximum at 93.5cm for ease of visualization (blue); V_m ramp computed via the estimated synaptic plasticity rule per cell (black); Each panel contains data from an individual place cell. **B)** Plot of V_m ramp widths computed for each individual place cell versus actual width for inferred rule (blue) and the 50 fold shorter rule (red).

Fig. S4. Robustness of plasticity rule estimate. A) Average synaptic rule across cells, with single cell kernels normalized by their temporal average in the [-5,5]s window as in Fig 2e (left), single cell kernels normalized by their peak in the same time window (center), and non-normalized (right). **B)** Correlation coefficient between the experimental V_m ramp width and the inferred V_m ramp width, estimated from single cell kernels, for varying concentration parameters k (width of CA3 place field input) and regularization parameter β.

Fig. S5. Dual plasticity signal time scales and resulting V_m **ramps from computational model of behavioral time scale plasticity. A-B)** The time scales of local **(A)** and global **(B)** plasticity signals were optimized to fit data from each experimental cell (grey, mean in black). Longer time scales than predicted by standard STDP rules were required to fit the data. **C-D)** Example experimental and model V_m ramps for one experimentally induced **(C)** and one naturally-occurring **(D)** place field.

Fig. S6. Behavioral time scale synaptic plasticity; individual recordings. A) Sketch of pairing protocol. **B**) plots of relative EPSP amplitude for individual neurons for each pairing interval as labeled. None is synaptic stimulation alone.

Fig. S7. Behavioral time scale synaptic plasticity: **grouped data. A)** pair of EPSPs used to determine synaptic strength (50 ms interval). Black trace is average baseline EPSP (30 traces prior to induction), red trace is average post-pairing EPSP (15 traces surrounding 20 mins post induction). Hyperpolarization following EPSPs from 50 ms, -25 pA current injection used to determine Rin. **B)** V_m trace showing representative induction protocol with 10 synaptic stimuli (20 Hz) followed by plateau potential (300 ms current injection). **C)** Average EPSP amplitude (normalized to baseline; ±sem) for population of neurons that received the indicated induction protocol. Induction (5 pairings) at 0 mins. Grey line is average EPSP amplitude for synaptic stimulation alone. Different pairing intervals are indicated (from top to bottom induction intervals are decreasing, negative values indicating synaptic stimulation followed by plateau). **D-F)** same as above but for induction protocols where synaptic stimulation followed plateau initiation (positive values). Average amplitude values binned for indicated intervals (D).

Fig. S8. BTSP is pathway-specific. A) pair of EPSPs used to determine synaptic strength (50 ms interval). Test path stimuli delivered firs and then control path stimuli. Black trace is average baseline EPSP (30 traces prior to induction), red trace is average post-pairing EPSP (15 traces surrounding 20 mins post induction). Hyperpolarization following EPSPs from 50 ms, -25 pA current injection used to determine Rin. **B)** Plot of EPSP amplitude for test (red) and control (black) from single neuron. **C)** Average test pathway EPSP amplitude (normalized to baseline) for population of neurons that received the induction protocol (black). Grey lines normalized test EPSP amplitude for each individual neuron. **D)** Same as C) except for control path. **E)** Average EPSP amplitudes (±SEM; n=6) for population of test pathway (red) and control pathway (black). *-p=0.0005; ns-p=0.23.

Fig. S9. BTSP produces predictive place fields. A) from top, sketch of mouse on linear track for one lap (lap 10) when plateau potential is initiated at location near particular feature (~100 cm), heat map of AP rate versus position (cm), set of gaussian functions represents tuned input from a set of CA3 neurons where height indicates weight (+), a constant level of un-tuned inhibition (-) counters unpotentiated excitation. **B)** Same as above for next and subsequent laps. Asymmetric seconds long plasticity rule produces place field firing that precedes the location of the plateau initiation site because the largest changes in the input weights are for CA3 place cells that active at these earlier positions (gaussians at 20-80 cm vs 100-120 cm). A steady level of un-tuned inhibition is unchanged (-, bottom).

fig. S1

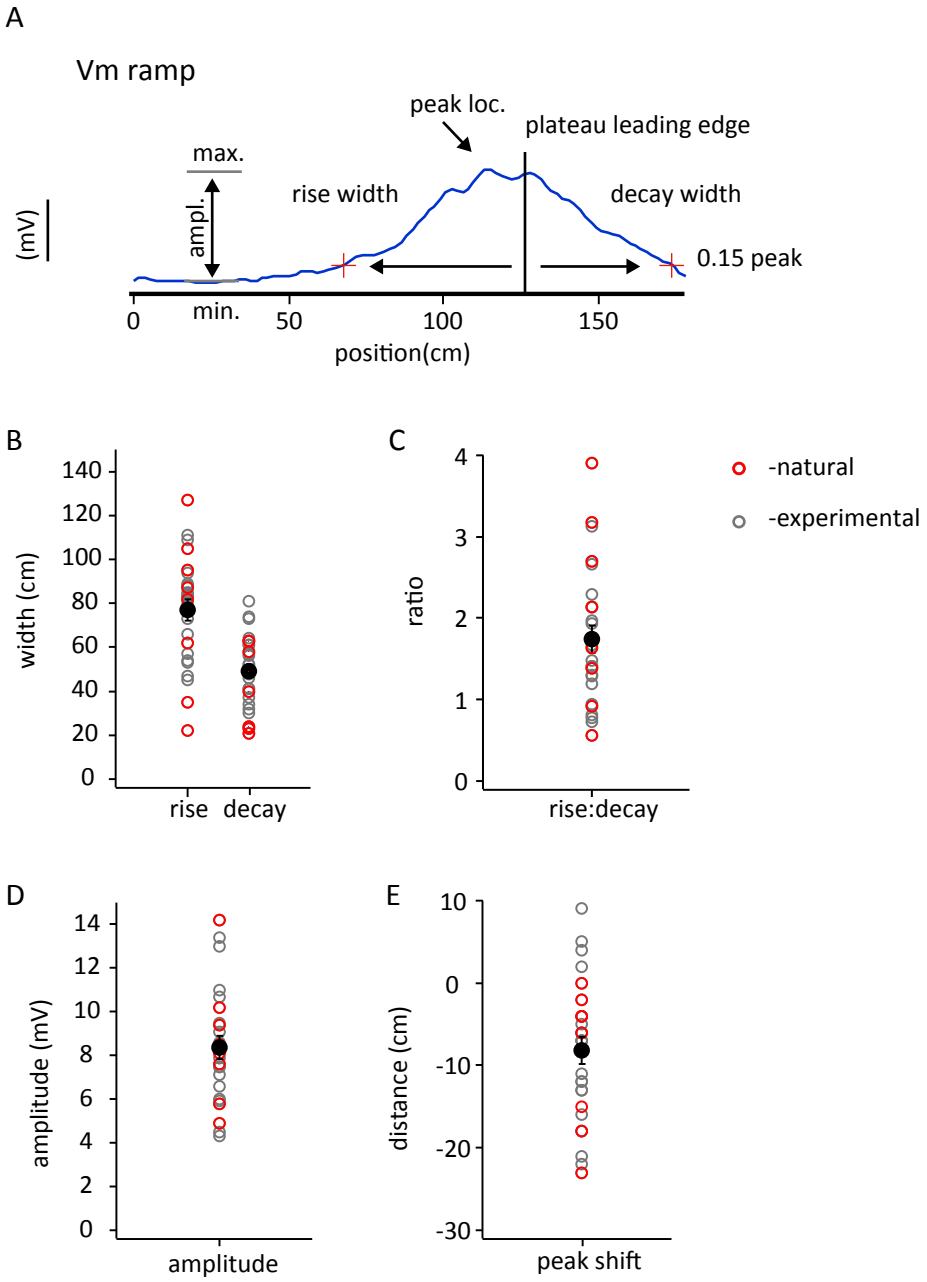

F

	Rise (cm)	Decay(cm)	ratio	Amplitude(mV)	Peak shift (cm)
All	76.77±4.94	49.27±3.27	1.74±0.17	8.38±0.52	-8.19±1.70
Experimental	76.72±4.89	52.22±3.76	1.61±0.17	8.29±0.64	-8.94±2.06
Natural	76.88±12.50	42.63±6.43	2.05±0.41	8.59±1.01	-6.50±3.31
P value	0.99	0.17	0.22	0.80	0.51

fig. S2

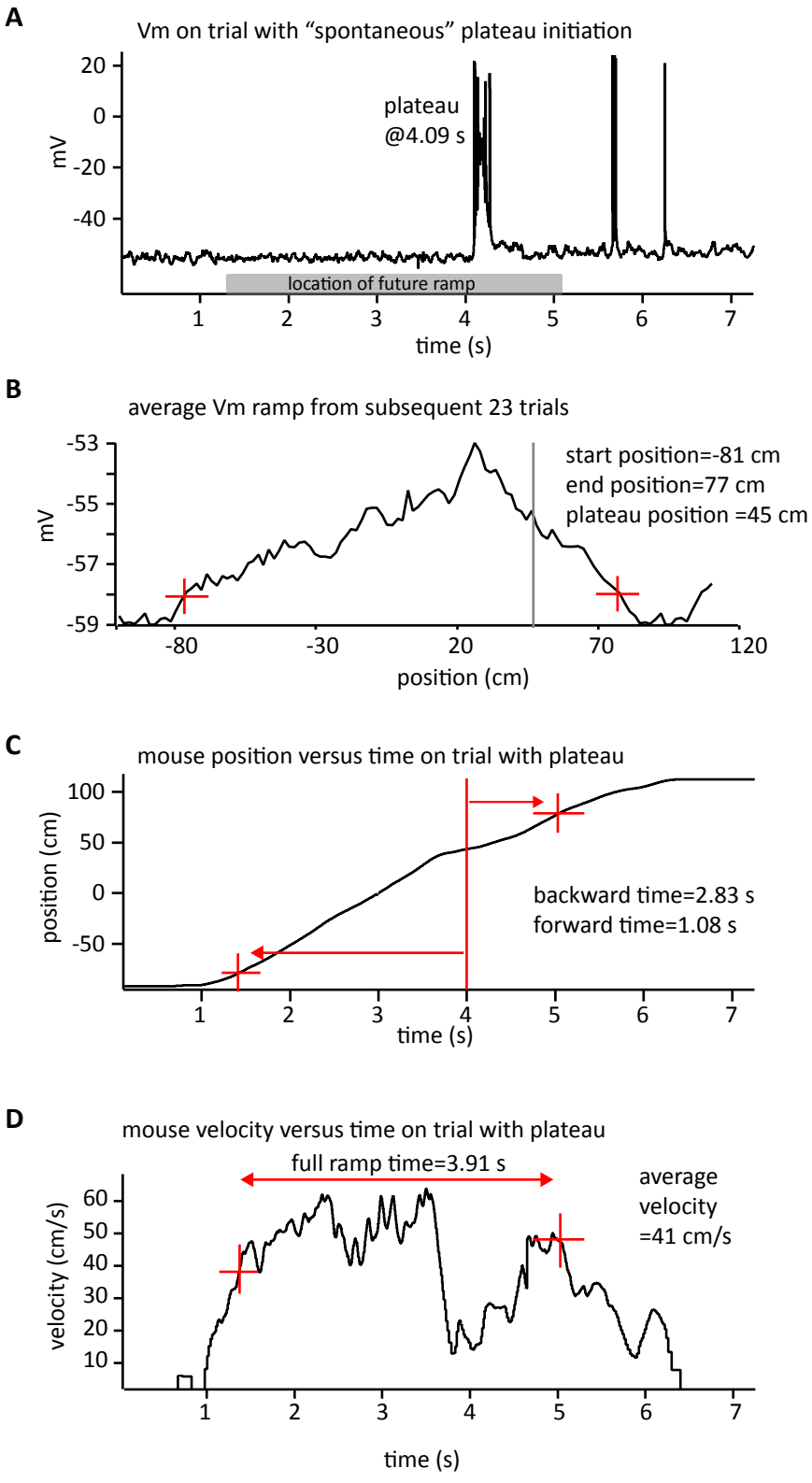
A
Vm on trial with “spontaneous” plateau initiation
plateau
@4.09 s
location of future ramp
mV
time (s)
B
average Vm ramp from subsequent 23 trials
start position=-81 cm
end position=77 cm
plateau position =45 cm
mV
position (cm)
C
mouse position versus time on trial with plateau
backward time=2.83 s
forward time=1.08 s
position (cm)
time (s)
D
mouse velocity versus time on trial with plateau
full ramp time=3.91 s
average
velocity
=41 cm/s
velocity (cm/s)
time (s)

fig. S3

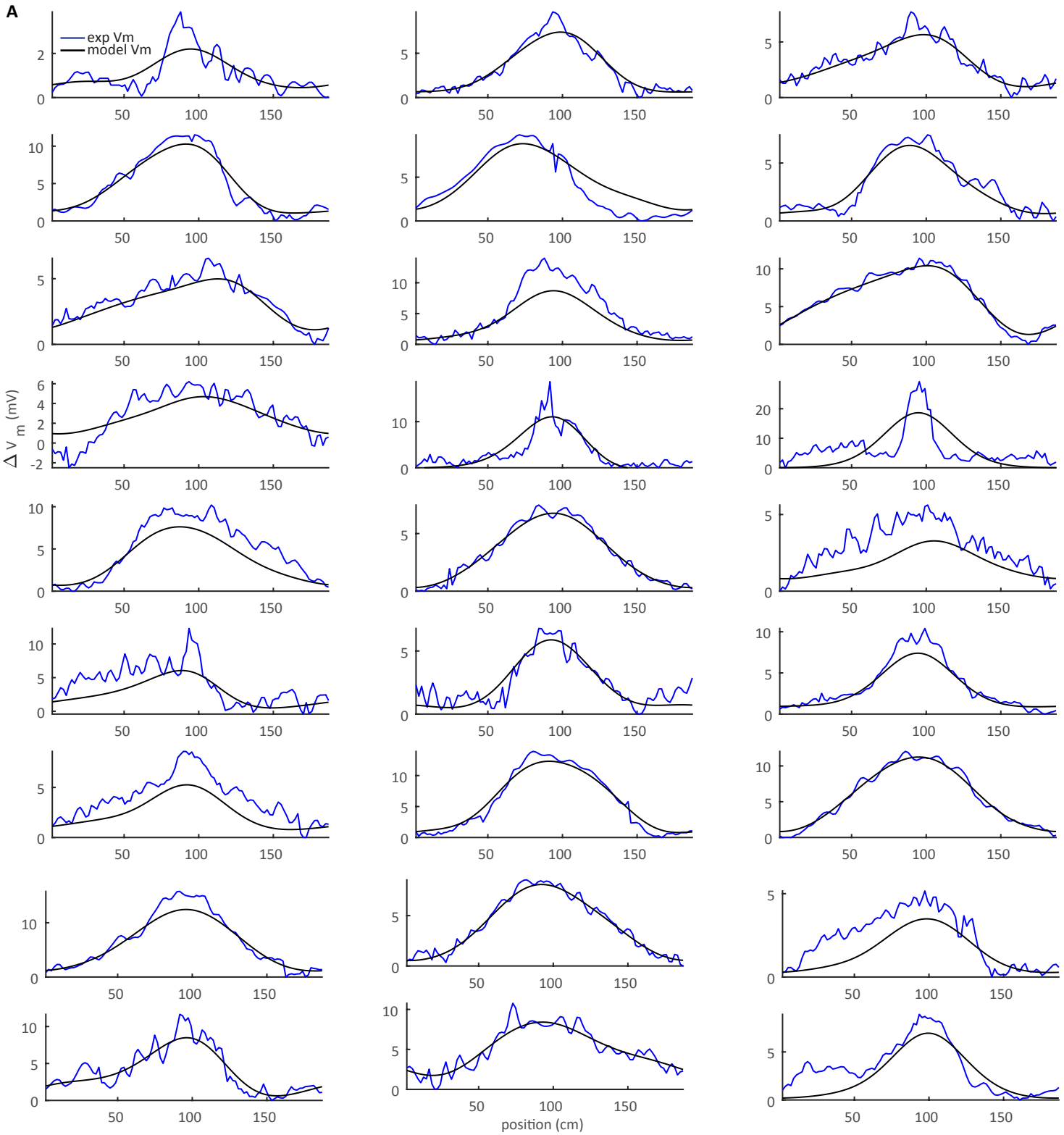
A
exp Vm
model Vm
Δ V m (mV)
position (cm)
B
plasticity rule
short rule
model Vm width (cm)
Vm width (cm)

fig. S4

A

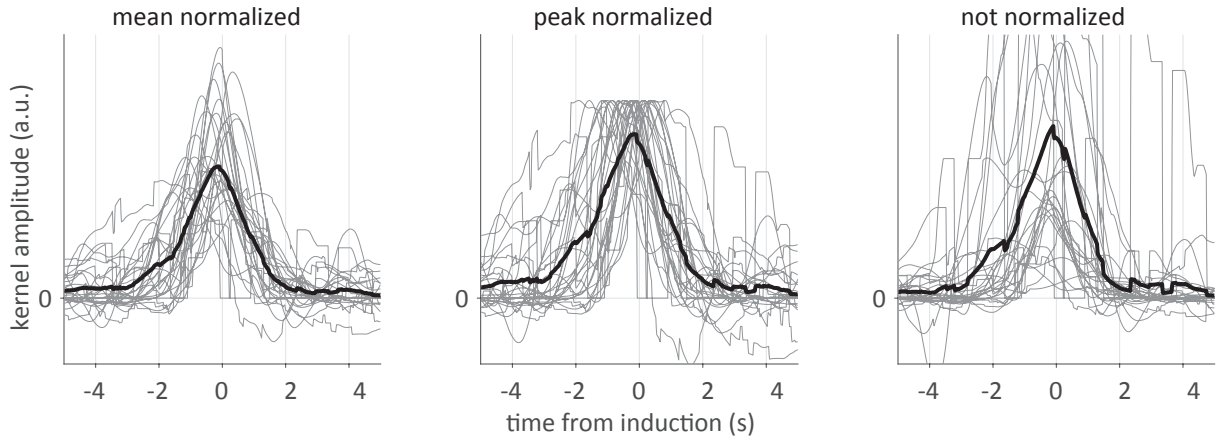
mean normalized
peak normalized
not normalized
kernel amplitude (a.u.)
0
-4
-2
0
2
4
time from induction (s)

B

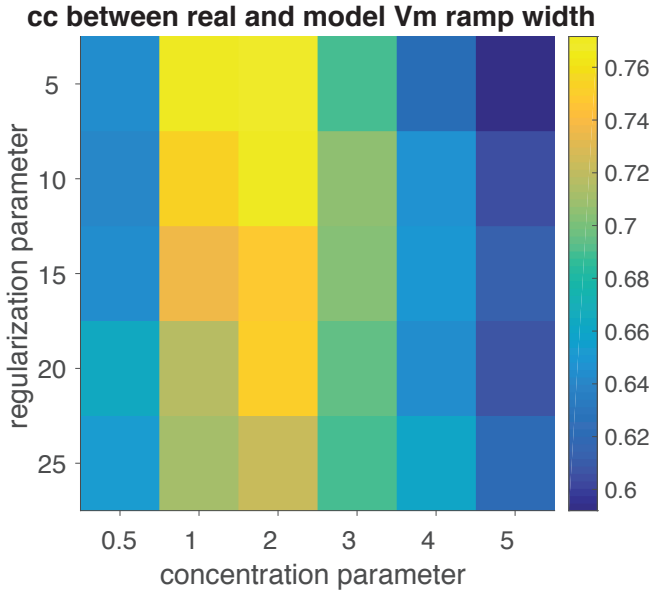
cc between real and model Vm ramp width
regularization parameter
5
10
15
20
25
concentration parameter
0.5
1
2
3
4
5
0.76
0.74
0.72
0.7
0.68
0.66
0.64
0.62
0.6

fig. S5

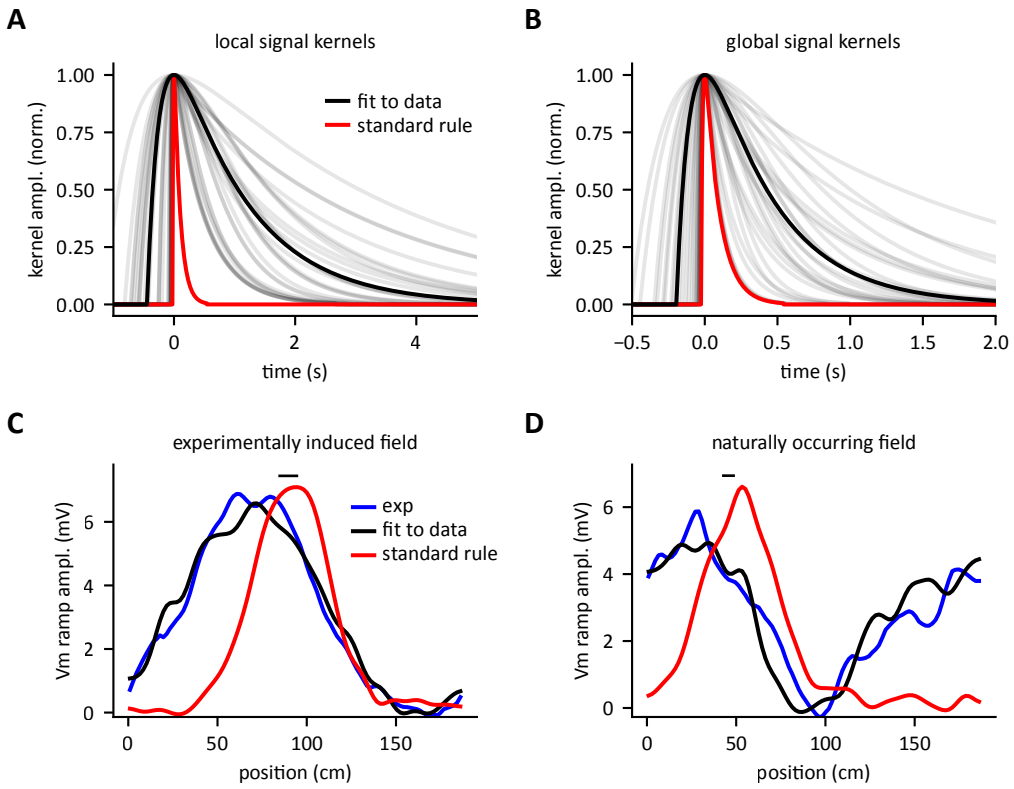
A
local signal kernels
fit to data
standard rule
kernel ampl. (norm.)
1.00
0.75
0.50
0.25
0.00
0
2
4
time (s)
B
global signal kernels
kernel ampl. (norm.)
1.00
0.75
0.50
0.25
0.00
−0.5
0.0
0.5
1.0
1.5
2.0
time (s)
C
experimentally induced field
exp
fit to data
standard rule
Vm ramp ampl. (mV)
6
4
2
0
0
50
100
150
position (cm)
D
naturally occurring field
Vm ramp ampl. (mV)
6
4
2
0
0
50
100
150
position (cm)

fig. S6

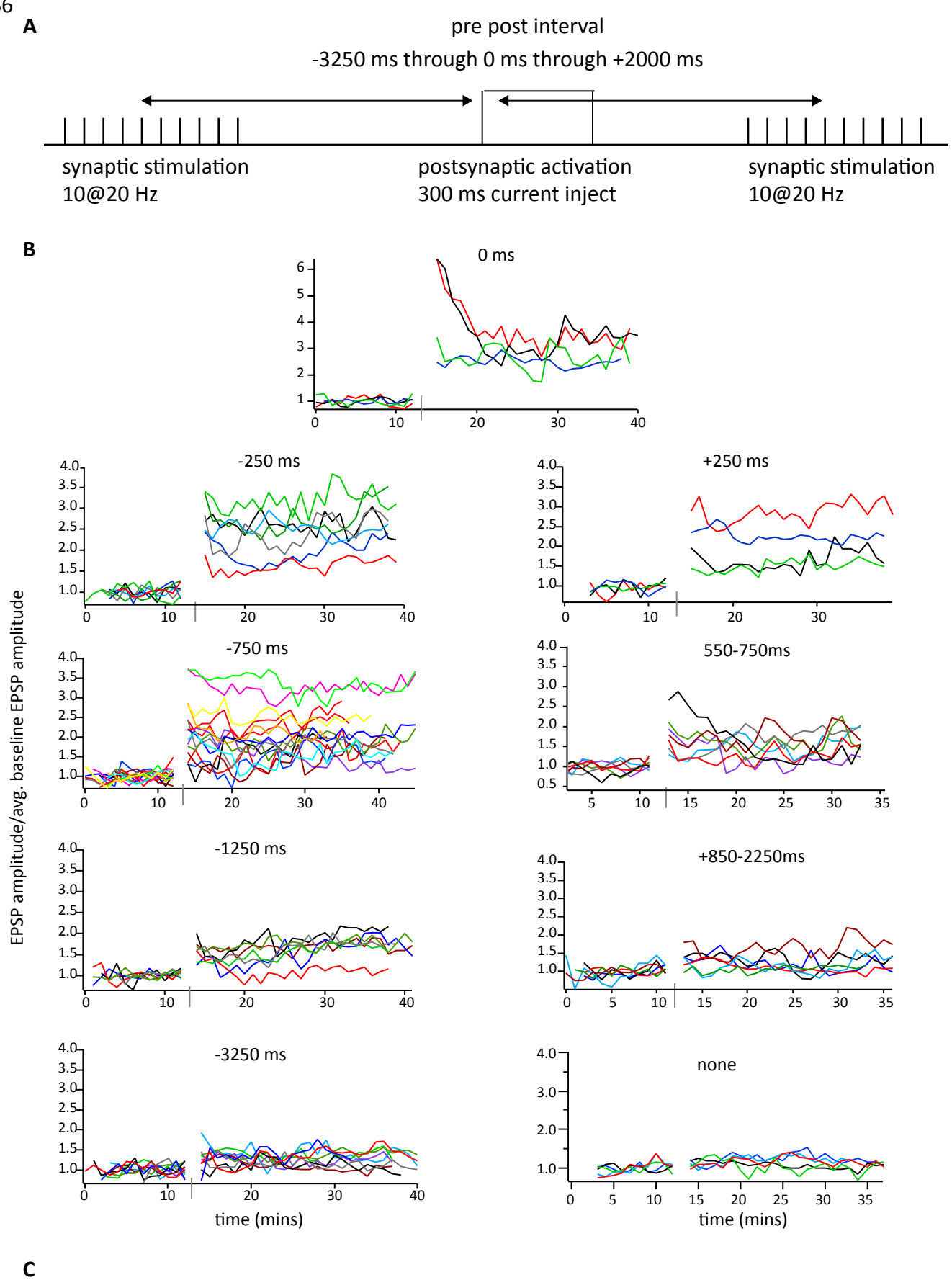
A
pre post interval
-3250 ms through 0 ms through +2000 ms
synaptic stimulation
10@20 Hz
postsynaptic activation
300 ms current inject
synaptic stimulation
10@20 Hz
B
0 ms
-250 ms
+250 ms
-750 ms
550-750ms
-1250 ms
+850-2250ms
-3250 ms
none
EPSP amplitude/avg. baseline EPSP amplitude
time (mins)
time (mins)
C
-750 ms
time (mins)

fig. S7

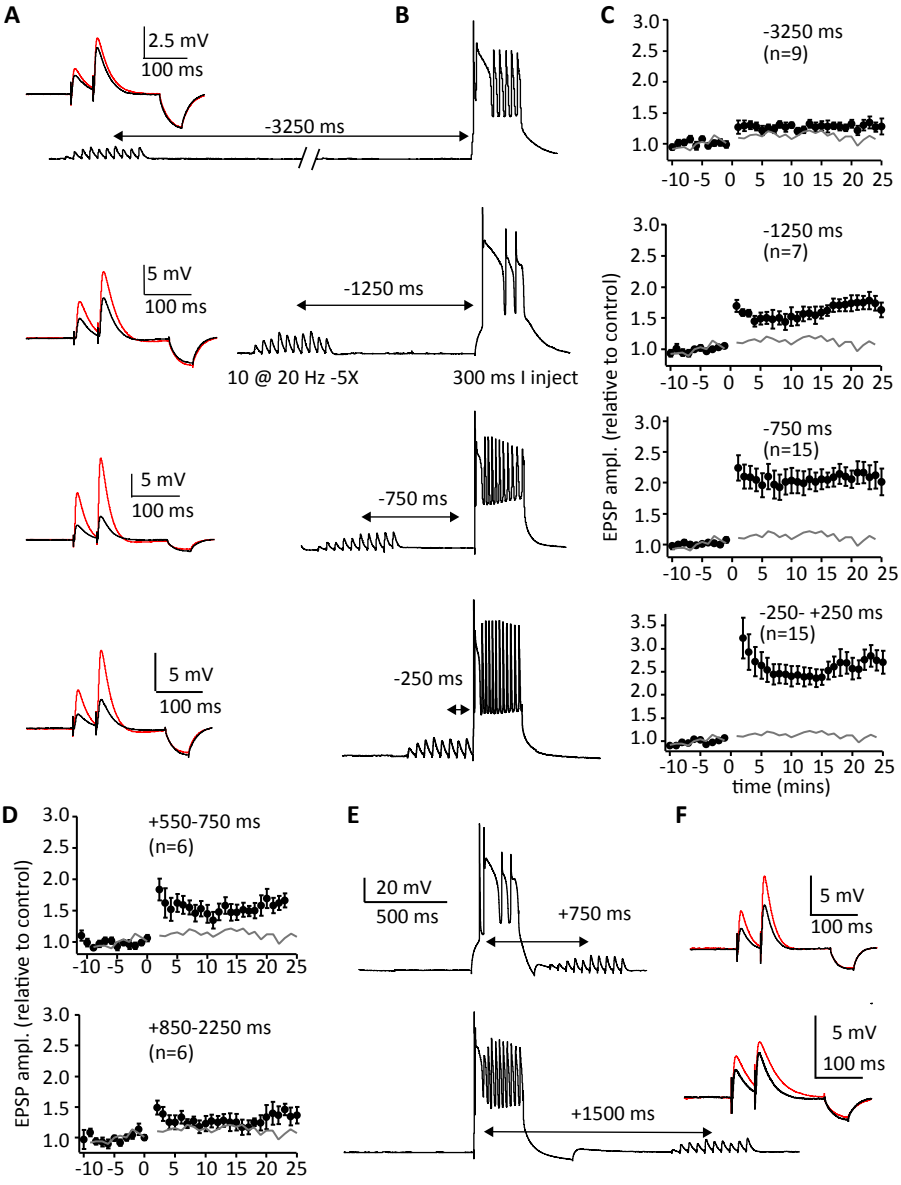
A
B
C
2.5 mV
100 ms
-3250 ms
-3250 ms
(n=9)
5 mV
100 ms
-1250 ms
10 @ 20 Hz -5X
300 ms I inject
-1250 ms
(n=7)
5 mV
100 ms
-750 ms
-750 ms
(n=15)
EPSP ampl. (relative to control)
5 mV
100 ms
-250 ms
-250- +250 ms
(n=15)
time (mins)
D
E
F
+550-750 ms
(n=6)
20 mV
500 ms
+750 ms
5 mV
100 ms
EPSP ampl. (relative to control)
+850-2250 ms
(n=6)
+1500 ms
5 mV
100 ms

fig. S8

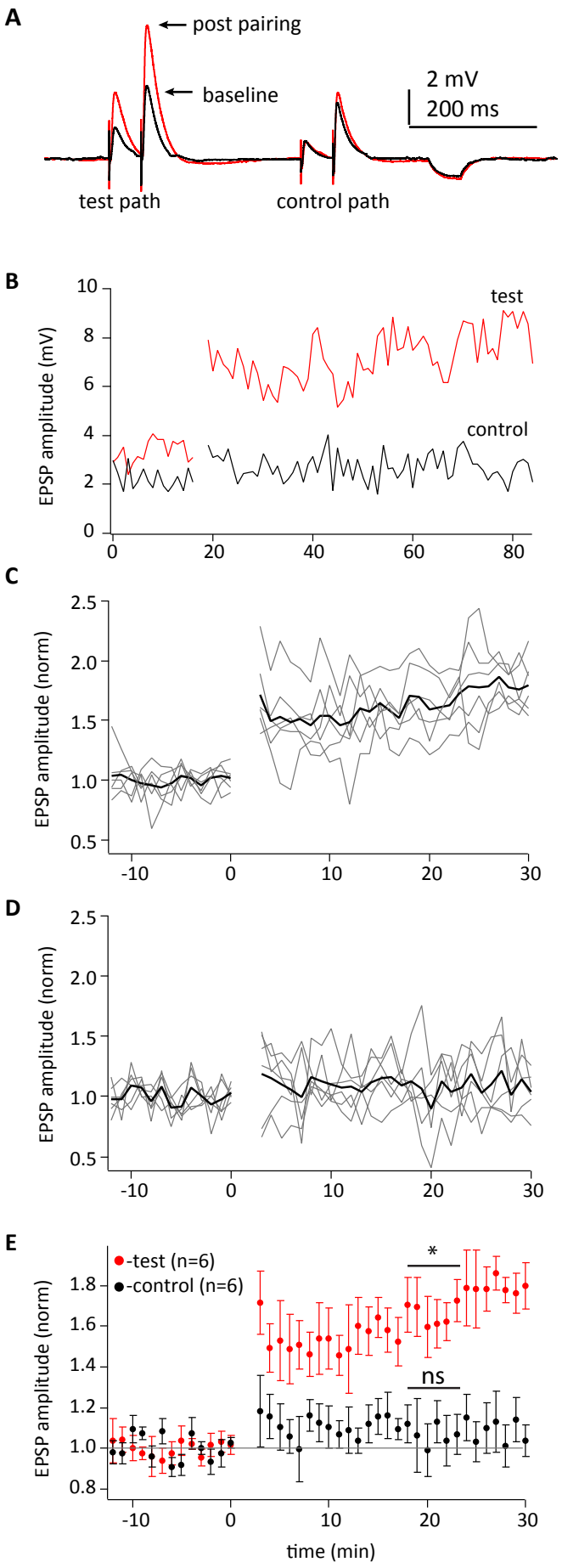
A
post pairing
baseline
2 mV
200 ms
test path
control path
B
EPSP amplitude (mV)
test
control
C
EPSP amplitude (norm)
D
EPSP amplitude (norm)
E
-test (n=6)
-control (n=6)
*
ns
EPSP amplitude (norm)
time (min)

fig. S9

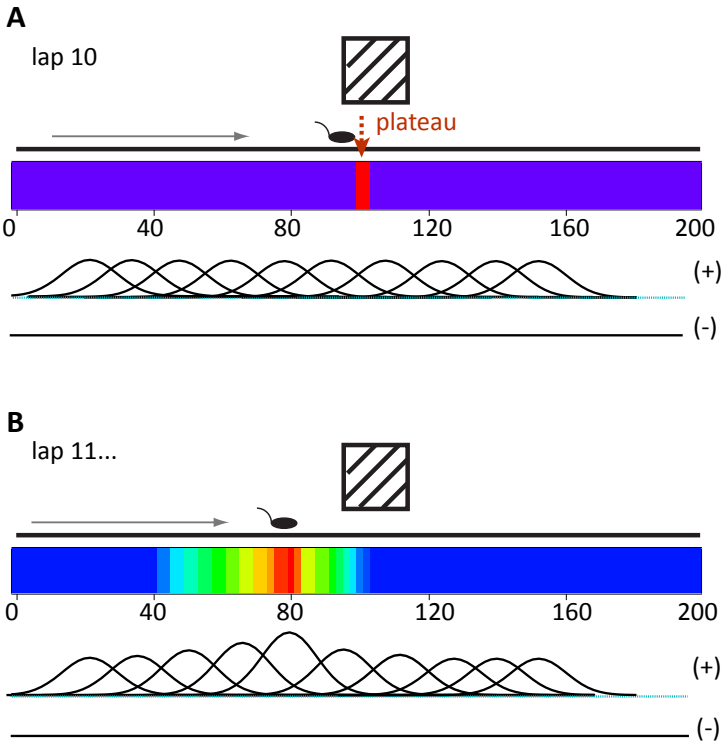

References and Notes

1. D. O. Hebb, *The Organization of Behavior* (Wiley, 1949).

2. R. S. Sutton, A. G. Barto, Toward a modern theory of adaptive networks: Expectation and prediction. *Psychol. Rev.* **88**, 135–170 (1981). doi:10.1037/0033-295X.88.2.135 Medline

3. P. Dayan, L. Abbott, *Theoretical Neuroscience* (MIT Press, 2001)

4. M. Mayford, S. A. Siegelbaum, E. R. Kandel, Synapses and memory storage. *Cold Spring Harb. Perspect. Biol.* **4**, a005751 (2012). doi:10.1101/cshperspect.a005751 Medline

5. D. E. Feldman, The spike-timing dependence of plasticity. *Neuron* **75**, 556–571 (2012). doi:10.1016/j.neuron.2012.08.001 Medline

6. T. V. Bliss, T. Lomo, Long-lasting potentiation of synaptic transmission in the dentate area of the anaesthetized rabbit following stimulation of the perforant path. *J. Physiol.* **232**, 331–356 (1973). doi:10.1113/jphysiol.1973.sp010273 Medline

7. K. I. Blum, L. F. Abbott, A model of spatial map formation in the hippocampus of the rat. *Neural Comput.* **8**, 85–93 (1996). doi:10.1162/neco.1996.8.1.85 Medline

8. J. C. Magee, D. Johnston, A synaptically controlled, associative signal for Hebbian plasticity in hippocampal neurons. *Science* **275**, 209–213 (1997). doi:10.1126/science.275.5297.209 Medline

9. H. Markram, J. Lübke, M. Frotscher, B. Sakmann, Regulation of synaptic efficacy by coincidence of postsynaptic APs and EPSPs. *Science* **275**, 213–215 (1997). doi:10.1126/science.275.5297.213 Medline

10. D. J. Foster, R. G. M. Morris, P. Dayan, A model of hippocampally dependent navigation, using the temporal difference learning rule. *Hippocampus* **10**, 1–16 (2000). doi:10.1002/(SICI)1098-1063(2000)10:1<1:AID-HIPO1>3.0.CO;2-1 Medline

11. E. M. Izhikevich, Solving the distal reward problem through linkage of STDP and dopamine signaling. *Cereb. Cortex* **17**, 2443–2452 (2007). doi:10.1093/cercor/bhl152 Medline

12. S. Cassenaer, G. Laurent, Conditional modulation of spike-timing-dependent plasticity for olfactory learning. *Nature* **482**, 47–52 (2012). doi:10.1038/nature10776 Medline

13. C. L. Hull, *Principles of Behavior* (Appleton-Century, New York, 1943).

14. P. R. Montague, P. Dayan, T. J. Sejnowski, A framework for mesencephalic dopamine systems based on predictive Hebbian learning. *J. Neurosci.* **16**, 1936–1947 (1996). Medline

15. P. J. Drew, L. F. Abbott, Extending the effects of spike-timing-dependent plasticity to behavioral timescales. *Proc. Natl. Acad. Sci. U.S.A.* **103**, 8876–8881 (2006). doi:10.1073/pnas.0600676103 Medline

16. W. B. Scoville, B. Milner, Loss of recent memory after bilateral hippocampal lesions. *J. Neurol. Neurosurg. Psychiatry* **20**, 11–21 (1957). doi:10.1136/jnnp.20.1.11 Medline

17. L. R. Squire, Memory systems of the brain: A brief history and current perspective. *Neurobiol. Learn. Mem.* **82**, 171–177 (2004). doi:10.1016/j.nlm.2004.06.005 Medline

18. D. Foster, J. Knierim, Sequence learning and the role of the hippocampus in rodent navigation. *Curr. Opin. Neurobiol.* **22**, 294–300 (2012). doi:10.1016/j.conb.2011.12.005 Medline

19. K. C. Bittner, C. Grienberger, S. P. Vaidya, A. D. Milstein, J. J. Macklin, J. Suh, S. Tonegawa, J. C. Magee, Conjunctive input processing drives feature selectivity in hippocampal CA1 neurons. *Nat. Neurosci.* **18**, 1133–1142 (2015). doi:10.1038/nn.4062 Medline

20. C. Grienberger, A. D. Milstein, K. C. Bittner, S. Romani, J. C. Magee, Inhibitory suppression of heterogeneously tuned excitation enhances spatial coding in CA1 place cells. *Nat. Neurosci.* **20**, 417–426 (2017). doi:10.1038/nn.4486 Medline

21. C. D. Harvey, F. Collman, D. A. Dombeck, D. W. Tank, Intracellular dynamics of hippocampal place cells during virtual navigation. *Nature* **461**, 941–946 (2009). doi:10.1038/nature08499 Medline

22. D. Lee, B.-J. Lin, A. K. Lee, Hippocampal place fields emerge upon single-cell manipulation of excitability during behavior. *Science* **337**, 849–853 (2012). doi:10.1126/science.1221489 Medline

23. K. Mizuseki, S. Royer, K. Diba, G. Buzsáki, Activity dynamics and behavioral correlates of CA3 and CA1 hippocampal pyramidal neurons. *Hippocampus* **22**, 1659–1680 (2012). doi:10.1002/hipo.22002 Medline

24. C. Geisler, D. Robbe, M. Zugaro, A. Sirota, G. Buzsáki, Hippocampal place cell assemblies are speed-controlled oscillators. *Proc. Natl. Acad. Sci. U.S.A.* **104**, 8149–8154 (2007). doi:10.1073/pnas.0610121104 Medline

25. H. Takahashi, J. C. Magee, Pathway interactions and synaptic plasticity in the dendritic tuft regions of CA1 pyramidal neurons. *Neuron* **62**, 102–111 (2009). doi:10.1016/j.neuron.2009.03.007 Medline

26. C. Kentros, E. Hargreaves, R. D. Hawkins, E. R. Kandel, M. Shapiro, R. V. Muller, Abolition of long-term stability of new hippocampal place cell maps by NMDA receptor blockade. *Science* **280**, 2121–2126 (1998). doi:10.1126/science.280.5372.2121 Medline

27. S. Remy, N. Spruston, Dendritic spikes induce single-burst long-term potentiation. *Proc. Natl. Acad. Sci. U.S.A.* **104**, 17192–17197 (2007). doi:10.1073/pnas.0707919104 Medline

28. C. D. Harvey, R. Yasuda, H. Zhong, K. Svoboda, The spread of Ras activity triggered by activation of a single dendritic spine. *Science* **321**, 136–140 (2008). doi:10.1126/science.1159675 Medline

29. S. J. Lee, Y. Escobedo-Lozoya, E. M. Szatmari, R. Yasuda, Activation of CaMKII in single dendritic spines during long-term potentiation. *Nature* **458**, 299–304 (2009). doi:10.1038/nature07842 Medline

30. B. Li, M. R. Tadross, R. W. Tsien, Sequential ionic and conformational signaling by calcium channels drives neuronal gene expression. *Science* **351**, 863–867 (2016). doi:10.1126/science.aad3647 Medline

31. S. A. Hollup, S. Molden, J. G. Donnett, M.-B. Moser, E. I. Moser, Accumulation of hippocampal place fields at the goal location in an annular watermaze task. *J. Neurosci.* **21**, 1635–1644 (2001). Medline

32. D. Dupret, J. O'Neill, B. Pleydell-Bouverie, J. Csicsvari, The reorganization and reactivation of hippocampal maps predict spatial memory performance. *Nat. Neurosci.* **13**, 995–1002 (2010). doi:10.1038/nn.2599 Medline

33. B. E. Pfeiffer, D. J. Foster, Hippocampal place-cell sequences depict future paths to remembered goals. *Nature* **497**, 74–79 (2013). doi:10.1038/nature12112 Medline

34. A. Sarel, A. Finkelstein, L. Las, N. Ulanovsky, Vectorial representation of spatial goals in the hippocampus of bats. *Science* **355**, 176–180 (2017). doi:10.1126/science.aak9589 Medline

35. D. G. Lavond, J. J. Kim, R. F. Thompson, Mammalian brain substrates of aversive classical conditioning. *Annu. Rev. Psychol.* **44**, 317–342 (1993). doi:10.1146/annurev.ps.44.020193.001533 Medline

36. H. Eichenbaum, Time cells in the hippocampus: A new dimension for mapping memories. *Nat. Rev. Neurosci.* **15**, 732–744 (2014). doi:10.1038/nrn3827 Medline

37. M. L. Hines, A. P. Davison, E. Muller, NEURON and Python. *Front. Neuroinform.* **3**, 1 (2009). doi:10.3389/neuro.11.001.2009 Medline

38. A. D. Milstein, Biophysically detailed CA1 place cell simulation code repository (2017); http://github.com/neurosutras/CA1Sim/tree/BTSP.